SMAP Detects Soil Moisture Under Temperate Forest Canopies

Geophysical Research Letters

RESEARCH LETTER
10.1029/2020GL089697

SMAP Detects Soil Moisture Under Temperate Forest Canopies

Andreas Colliander[1], Michael H. Cosh[2], Vicky R. Kelly[3], Simon Kraatz[4], Laura Bourgeau-Chavez[5], Paul Siqueira[4], Alexandre Roy[6], Alexandra G. Konings[7], Natan Holtzman[7], Sidharth Misra[1], Dara Entekhabi[8], Peggy O'Neill[9], and Simon H. Yueh[1]

[1]Jet Propulsion Laboratory, California Institute of Technology, Pasadena, CA, USA, [2]USDA ARS Hydrology and Remote Sensing Laboratory, Beltsville, MD, USA, [3]Cary Institute of Ecosystem Studies, Millbrook, NY, USA, [4]Electrical and Computer Engineering, University of Massachusetts Amherst, Amherst, MA, USA, [5]Michigan Tech Research Institute, Ann Arbor, MI, USA, [6]Département des Sciences de l'Environnement, Université du Québec à Trois-Rivières, Trois-Rivières, Québec, Canada, [7]Department of Earth System Science, Stanford University, Stanford, CA, USA, [8]Department of Earth, Atmospheric and Planetary Sciences, Massachusetts Institute of Technology, Cambridge, MA, USA, [9]NASA Goddard Space Flight Center, Greenbelt, MD, USA

Abstract Soil moisture dynamics in the presence of dense vegetation canopies are determinants of ecosystem function and biogeochemical cycles, but the capability of existing spaceborne sensors to support reliable and useful estimates is not known. New results from a recently initiated field experiment in the northeast United States show that the National Aeronautics and Space Administration (NASA) SMAP (Soil Moisture Active Passive) satellite is capable of retrieving soil moisture under temperate forest canopies. We present an analysis demonstrating that a parameterized emission model with the SMAP morning overpass brightness temperature resulted in a RMSD (root-mean-square difference) range of 0.047–0.057 m^3/m^3 and a Pearson correlation range of 0.75–0.85 depending on the experiment location and the SMAP polarization. The inversion approach included a minimal amount of ancillary data. This result demonstrates unequivocally that spaceborne L-band radiometry is sensitive to soil moisture under temperate forest canopies, which has been uncertain because of lack of representative reference data.

Key Points:
- Soil moisture monitoring networks were deployed at two forested sites for SMAP validation experiment
- SMAP brightness temperature was used to retrieve soil moisture over predominantly forested sites
- The study demonstrates the capability of spaceborne L-band radiometry to retrieve soil moisture under forest canopies

Supporting Information:
- Supporting Information S1

Correspondence to:
A. Colliander,
andreas.colliander@jpl.nasa.gov

Citation:
Colliander, A., Cosh, M. H., Kelly, V. R., Kraatz, S., Bourgeau-Chavez, L., Siqueira, P., et al. (2020). SMAP detects soil moisture under temperate forest canopies. *Geophysical Research Letters*, *47*, e2020GL089697. https://doi.org/10.1029/2020GL089697

Received 3 JUL 2020
Accepted 17 SEP 2020
Accepted article online 21 SEP 2020

1. Introduction

During times of low soil moisture availability, trees experience water stress whereby their ability to maintain hydraulic integrity and continue physiological function becomes limited (Choat et al., 2012; Corlett, 2016; Doughty et al., 2015). Mapping the available water in the soils of these ecosystems is restricted by the effects of the canopy that stands between the remote sensing instrument and the forest floor. Remote sensing of soil moisture in forested areas has been an elusive goal since the start of microwave remote sensing, while for nonforested areas soil moisture data are being provided routinely (e.g., Chan et al., 2016, 2018; Das et al., 2019; Dorigo et al., 2017; Kerr et al., 2016). Radiation emission and reflection from the soil surface in the lower-frequency range of the microwave region of the spectrum are less likely than higher frequencies (including optical) to lose usefulness for tracking soil moisture dynamics in the presence of attenuation and scattering by vegetation. Specifically, radiometer observations at L-band (within the 1- to 2-GHz band, a small subband centered at 1.413 GHz is reserved for space and Earth science) have long been considered to be more suitable for soil moisture detection than higher frequencies (Schmugge et al., 1986). Forests represent the extreme of vegetation density where the low frequency is considered to be critical for a potential soil moisture detection. In the past, a number of studies in fully or partially forested conditions included tower-based (e.g., Guglielmetti et al., 2008; Kurum et al., 2012) and airborne (e.g., Lang et al., 2001; Macelloni et al., 2001; McNairn et al., 2015; Seppanen et al., 2016) measurements with L-band radiometers. These studies showed mixed results for soil moisture sensitivity.

ESA (European Space Agency) launched a satellite carrying an L-band radiometer in 2009 called Soil Moisture Ocean Salinity (SMOS) (Mecklenburg et al., 2016) and NASA (National Aeronautics and Space Administration) in 2015 called Soil Moisture Active Passive (SMAP) (Entekhabi et al., 2010). These missions opened the door for wide scale retrieving of soil moisture in forested area from space (e.g., Djamai et al., 2015; Kang et al., 2016, 2019; Monsiváis-Huertero et al., 2020; Vittucci et al., 2016). However, the lack of

appropriate reference soil moisture sources has been a major obstacle for quantifying, developing, testing, and validating soil moisture retrieval algorithms from satellite observations (e.g., Vittucci et al., 2019).

Across nonforested or sparsely forested pixels, the performance of the SMAP radiometer-based soil moisture products meet the mission requirements as the requirements apply to conditions where the vegetation water content is less than typical forested areas (up to 5 kg/m^2) (Chan et al., 2016, 2018). The prevailing view is that above this level of canopy water content, the attenuation and scattering of surface emission by the vegetation are too strong to allow reliable inference about soil moisture. As the mission moved to the extended phase in June 2018, one of its objectives was to expand the domain of validated retrievals to forested areas. As the core sites used to validate the SMAP soil moisture retrieval performance did not include appropriate locations in forested environments (Colliander, Cosh, et al., 2017), the mission decided to conduct field experiments in forested regions. The first experiment, called SMAP Validation Experiment 2019–2021 (SMAPVEX19-21), started in 2019 in two locations in the northeastern United States and will continue through 2021. The experiment follows a series of SMAP postlaunch validation experiments conducted in biomes with predominantly lower vegetation water content (e.g., Colliander, Jackson, et al., 2017; Colliander et al., 2019). The objective of the experiment is to test the SMAP retrieval in both fully forested and partially forested areas because a substantial portion of the United States and the globe have a nonuniform forest cover at the SMAP resolution scale.

In this study, we present an analysis using the first-year station measurements of SMAPVEX19-21. Our hypothesis is that with a correctly parameterized emission model it is possible to retrieve soil moisture for the experiment domains. The parameterization of the low-frequency microwave emission from forests requires accounting for vegetation scattering in addition to vegetation attenuation and surface roughness. Several electromagnetic models have been presented in the past for accounting for the vegetation effect on the soil emission. The weakness of the widely used tau-omega model is that it assumes a low scattering for the vegetation in its formulation (Mo et al., 1982); this weakness has been addressed in many studies and alternative approaches have been presented (e.g., Ferrazzoli et al., 2002; Kurum et al., 2011; Schwank et al., 2018). The SMAP single channel algorithm (SCA) also uses the tau-omega model for vegetation compensation (O'Neill, Chan, Njoku, Jackson, & Bindlish, 2019). Here, we used one of the alternative models presented in Colliander et al. (2018) that do not approximate the scattering contribution. The model has essentially the same parameters as the tau-omega model and in the absence of vegetation scattering it produces identical results to the tau-omega model. We compare the retrieval results using the parameterized model with the station-measured values to investigate whether SMAP is sensitive to soil moisture at the forested experiment sites.

2. Materials and Methods

2.1. SMAPVEX19-21 Sites

The mission chose two locations for SMAPVEX19-21, each encompassing an area corresponding to the retrieval domain of the SMAP enhanced soil moisture product (about 33 km). Figure 1a shows the locations of the experiment sites in central Massachusetts and the Hudson Valley of New York. The Massachusetts (MA) site is 84% forested incorporating the Harvard Forest research site (https://harvardforest.fas.harvard.edu/) within its boundaries. The SMAP grid cell for MA has a dominance of beech-maple (~46%) followed by pine forest (~24%) and oak-hickory (~12%) based on the National Land Cover Database (NLCD). The grid cell also has about 13% wetlands (~12% forested, ~1% herbaceous) and only about 4% grassland/hay fields.

A permanent monitoring network of six soil moisture stations has been operating in upstate New York since 2015. The site is located near the village of Millbrook (MB) (Figure 1a). The site is about 36% nonforested, with about 23% of the total grid cell area mapped as pasture/hay fields by NLCD. Most of the forested station locations in the SMAP grid cell are oak-hickory (~30%) or beech-maple (~30%), with a few conifer forests (~4%).

The forests in the experiment domains are representative of the northeastern temperate forests. The regional (about 150-km area around the experiment domains) mean biomass is about 130 t/ha with a standard deviation of 70 t/ha based on the U.S. Forest Service Forest Inventory and Analysis data. The dominant species are

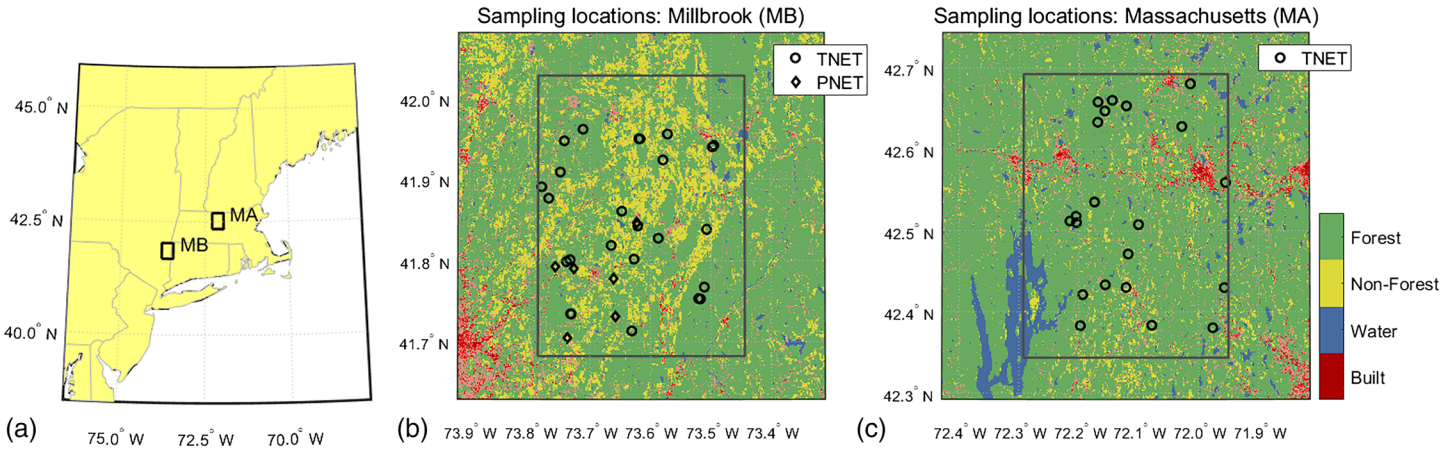

Figure 1. (a) Map of the experiment locations near Millbrook, New York (MB), and Amherst, Massachusetts (MA). (b) Locations of the temporary 25 soil moisture stations in the Millbrook pixel, and the locations of the six permanent stations (PNET) operated in the area. (c) Locations of the temporary 23 soil moisture stations (TNET) in the Massachusetts pixel. The background colors in (b) and (c) are based on the National Land Cover Database. The rectangles depict the SMAP pixel and the outlines of (b) and (c) are 50 km by 50 km.

Red and Sugar Maple, Red Oak, Eastern Hemlock, and Eastern White Pine, and other typical species are White Ash, American Beech, Black Birch, and Black Cherry based on the same data set. The biomass estimates and species composition found in local studies conducted at the experiment domains are mostly consistent with the regional characteristics. For example, Katz et al. (2010) show biomass values in the MB domain very close to the mean value of the region, while Ahmed et al. (2013) show that in the Harvard Forest area (which is not atypical in the MA domain) the biomass values may be on the high end of the regional values but within the range.

The experiment started by an installation of 23- and 25-station networks at the MA and MB sites in May 2019, respectively (Cosh et al., 2020a, 2020b). Figures 1b and 1c show the locations of the stations. In order to accurately determine the average soil moisture within the experiment domains, a sufficient number of sampling locations are needed to account for the spatial variability. However, the spatial variability of soil moisture is not known exactly over the domains. Studies have presented relationships between soil moisture spatial variability and the required number of sampling locations (e.g., Famiglietti et al., 2008) as well as uncertainty estimates for spatial means based on the variability (Chen et al., 2019). Based on the typical station numbers required in the previous studies (see also Crow et al., 2012), the number of sensors at each of the MA and MB sites should provide satisfactory accuracy for the average soil moisture estimate while respecting the logistical challenges for deploying the stations in forested landscapes.

The temporary network stations include soil moisture measurements with Stevens Water HydraProbe sensors at three different depths: one measuring a layer from the top down to about 6-cm depth, one measuring a layer at the depth of about 3–7 cm, and one a layer at the depth of about 8–12 cm. The first sensor is installed vertically top down, while the other two are installed horizontally. The soil moisture sensors at each depth also include a temperature sensor. Additionally, the stations include air temperature measurement at about 1.5-m height aboveground and a nadir pointing wildlife camera used for phenology monitoring. Some of the locations also include sap flow sensors and dielectric measurement of the tree trunks to enhance the vegetation monitoring (Matheny et al., 2015; Roy et al., 2020).

The factory calibration of the soil moisture sensors is not expected to provide unbiased soil moisture value because of the complex textural composition of the soil at the sites. The top layers of the soil are mixed with organic matter in different stages of decomposition. In this study, we used the measured real part of the dielectric constant (ε_r) as the reference. Two intensive observation periods planned for 2021 will include collection of soil core samples that will be used to eventually calibrate the soil moisture sensors using the thermogravimetric method (Dane & Topp, 2002). Before using the measurements, each sensor time series was checked to be sure it did not have anomalous behavior (spikes, steps, drifting, etc.) or data gaps that would affect the mean value computed for the domains.

2.2. SMAP Brightness Temperature Data

The L-band radiometer on-board the SMAP satellite includes vertically (V) and horizontally (H) polarized brightness temperature (TB) channels. The satellite has a Sun-synchronous 6 a.m./6 p.m. equator-crossing orbit, a constant 40° sensor incidence angle, and an approximately 1,000-km swath width, which results in global coverage every 2–3 days (Entekhabi et al., 2014). The measurements have about 38-km resolution (defined by the half-power footprint on the Earth's surface of the radiometer antenna pattern) and the radiometric resolution of the gridded SMAP TB is less than 0.5 K (Piepmeier et al., 2017). The SMAP enhanced TB and soil moisture products grid the values on a 9-km EASE Version 2 grid (Chaubell et al., 2019; O'Neill, Chan, Njoku, Jackson, Bindlish, & Chaubell, 2019). However, as the actual footprint of the measurement is considerably larger than the grid size, the retrieval domain for the enhanced soil moisture product was chosen to be about 33 km (Chan et al., 2018). The actual size is determined based on 11 by 11 cells of the SMAP 3-km grid, which is nested with the 9-km grid. Thus, the domains are not exactly square, but follow the shape of the EASE Version 2 grid used for SMAP (see Figure 1). The analysis presented here excluded the TB measurements flagged for radio frequency interference contamination (Mohammed et al., 2016; Piepmeier et al., 2014). The SMAP satellite experienced a data outage from 20 June to 22 July 2019 resulting in no retrievals during this period.

2.3. Forward Model

In order to model the forest emission, we applied a two-layer model introduced in Colliander et al. (2018). The model represents propagation of emission in the soil-vegetation-air medium with vegetation transmission (t_p; p stands for polarization, V or H) and scattering (S_p) parameters. The top of the vegetation TB is formulated as follows:

$$T_{Bp} = (1 - r_p) T_{soil} \left(\frac{t_p}{1 + S_p r_p} \right) + \left(1 - \frac{t_p}{1 - S_p} \right) T_{veg} + \left(1 - \frac{t_p}{1 - S_p} \right) T_{veg} \frac{t_p r_p}{1 + S_p r_p} \tag{1}$$

where T_{soil} is the effective temperature of the soil and T_{veg} is the effective temperature of the vegetation layer. Effective temperatures corresponds to the average temperature of the parts of the medium emitting the radiation (see, e.g., Njoku & Kong, 1977). The transmission, t_p, parameter is related to the vegetation optical (electromagnetic) depth parameter τ_p as follows:

$$t_p = e^{-\tau_p} \tag{2}$$

The scattering parameter (S_p) is related to the radiative transfer scattering coefficient (κ_{sp}) as

$$S_p = 1 - e^{-\kappa_{sp}} \tag{3}$$

Thus, the scattering albedo can be solved as $\omega_p = \kappa_{sp}/\tau_p$. It is noted that for the τ-ω model the τ and ω parameters are not exactly the same as defined in standard radiative transfer modeling although they serve a similar purpose (Mo et al., 1982). Finally, the vegetation absorption (a_p) is given by the $1 - t_p/(1 - S_p)$ component in 1. According to Kirchhoff's law, the absorption determines the emission by the vegetation. The three terms on the right-hand side of 1 represent from left to right: the soil emission through vegetation, vegetation emission, and vegetation emission reflected from the ground and propagated up through the vegetation, respectively.

We modeled the rough surface reflectivity (r_p) with an adaptation of the classical Choudhury roughness model (Choudhury et al., 1979), which with constant incidence angle reduces to a simple multiplicative factor (H_{0p}) on the Fresnel flat surface reflectivity (r_{0p}):

$$r_p = r_{0p} H_{0p} = r_{0p} e^{-H_p} = r_{0p} e^{-h_p \cos^2(\theta)} \tag{4}$$

where h_p is the original roughness parameter in the Choudhury model; H_p represents a normalized roughness parameter used later to compare the parameterization to literature values, and θ stands for incidence angle. We do not assume polarization mixing in the rough surface ($Q = 0$). The flat surface reflectivity is related to the ε_r of the soil through the Fresnel equations (e.g., Njoku & Entekhabi, 1996).

We transformed both the retrieved ε_r and the measured ε_r to soil moisture using the Mironov dielectric model (Mironov et al., 2009) in order to assess the results in the soil moisture scale. The use of the same model for the measured ε_r and the retrieved ε_r eliminates the additional uncertainty of potentially inaccurate and divergent dielectric models applied to the in situ sensors and the retrievals.

2.4. Parameter Optimization Approach

Our goal was to find a set of model parameters for predicting soil moisture from the SMAP measurements. Relatively little is known about the surface and vegetation parameterization at the global scale, in particular, for forests. The underrepresentation of the forested field campaigns in the past have led most retrieval algorithms to assume a set of values that is globally uniform or dependent on the land cover classification schemes that do not necessarily correspond to the real variability of these parameters. Similarly, because little is known of what T_{veg} should be, most algorithms assume the same value for T_{soil} and T_{veg} (and focus on retrieval times when the diurnally variable vertical temperature gradient is assumed to be smallest), but in taller and denser canopies, such as forests, this assumption is more likely to break down. The local optimization of the parameters will help us to answer the question of whether SMAP retrievals are possible but does not automatically translate to globally applicable parameters.

Essential for testing SMAP's skill to detect soil moisture changes is an adequate range of soil moisture during the test period. The first-year measurements of SMAPVEX19-21 provide a 0.35 m^3/m^3 range at the MA pixel and a 0.39 m^3/m^3 range at the MB pixel, which satisfies this requirement. For computing the reference soil ε_r, we averaged the measurements from the vertically installed sensors representing the spatial domain (see section 2.1). We inverted the forward model and simulated soil ε_r for the measured SMAP TB with different model parameter values. Thus, for each parameter combination, we had a set of inverted ε_r values corresponding to the measured TB, which we compared with respect to the station-measured ε_r. Moreover, we extended the optimization process to include the selection of temperature measurements for T_{soil} and T_{veg}. Each parameter combination was computed with different permutations of the measured temperatures as follows: T_{soil} was one of the temperatures measured by the soil moisture sensors, and T_{veg} was one of the temperatures measured by the soil moisture sensors or the air temperature.

We computed the RMSD (root-mean-square difference), mean difference (MD), and slope between the set of inverted and measured ε_r for each case with different parameter values and temperature selections. Each parameter was swept over a range of values and the metrics were computed for each case. Because it is possible to achieve the best RMSD with poor MD and/or slope, we set a limit for the MD and the slope and then picked the parameter values corresponding to the minimum RMSD within this subset. We executed this process separately for V and H polarization and the two experiment domains resulting in optimized H_p, t_p, and S_p parameters as well as a choice of temperature source for T_{soil} and T_{veg} for both domains. There is no reason to assume major seasonality for H_p. The t_p parameter may vary as a result of the water content changes in the trees over the season, especially as the domains are dominated by deciduous species, which may also affect S_p. The multiyear data set will provide a more robust basis for investigation of the seasonality of these parameters; here we focused on demonstrating the sensitivity to soil moisture variability.

3. Results

We performed the parameter optimization approach described in section 2.4 for the MA and MB domain. The slope limits for the parameter search were 1 ± 0.1, and the bias limits were ± 1 in ε_r. There was a fair amount of variability in the results, but we also observed that some cases with different combinations of the parameters resulted in relatively similar results. The results were also reasonably similar when we separated the SMAP morning (AM) and evening (PM) overpasses. Therefore, after some iteration we fixed the roughness parameter for V and H polarization and the choice of temperature measurement (see below) as we noticed that we could achieve essentially the same performance, but with more consistent parameterization across different cases. This helps the interpretation of the results. For the parameter search, we combined the AM and PM overpasses but computed the eventual metrics separately for the two cases.

Figure 2 shows the scatterplots in soil moisture for the retrievals over each domain using the SMAP vertically and horizontally polarized TB for AM and PM overpasses separately. The outliers marked with circle correspond to mostly PM overpass measurements very early in the season before leaf flush (Figure S1 in the

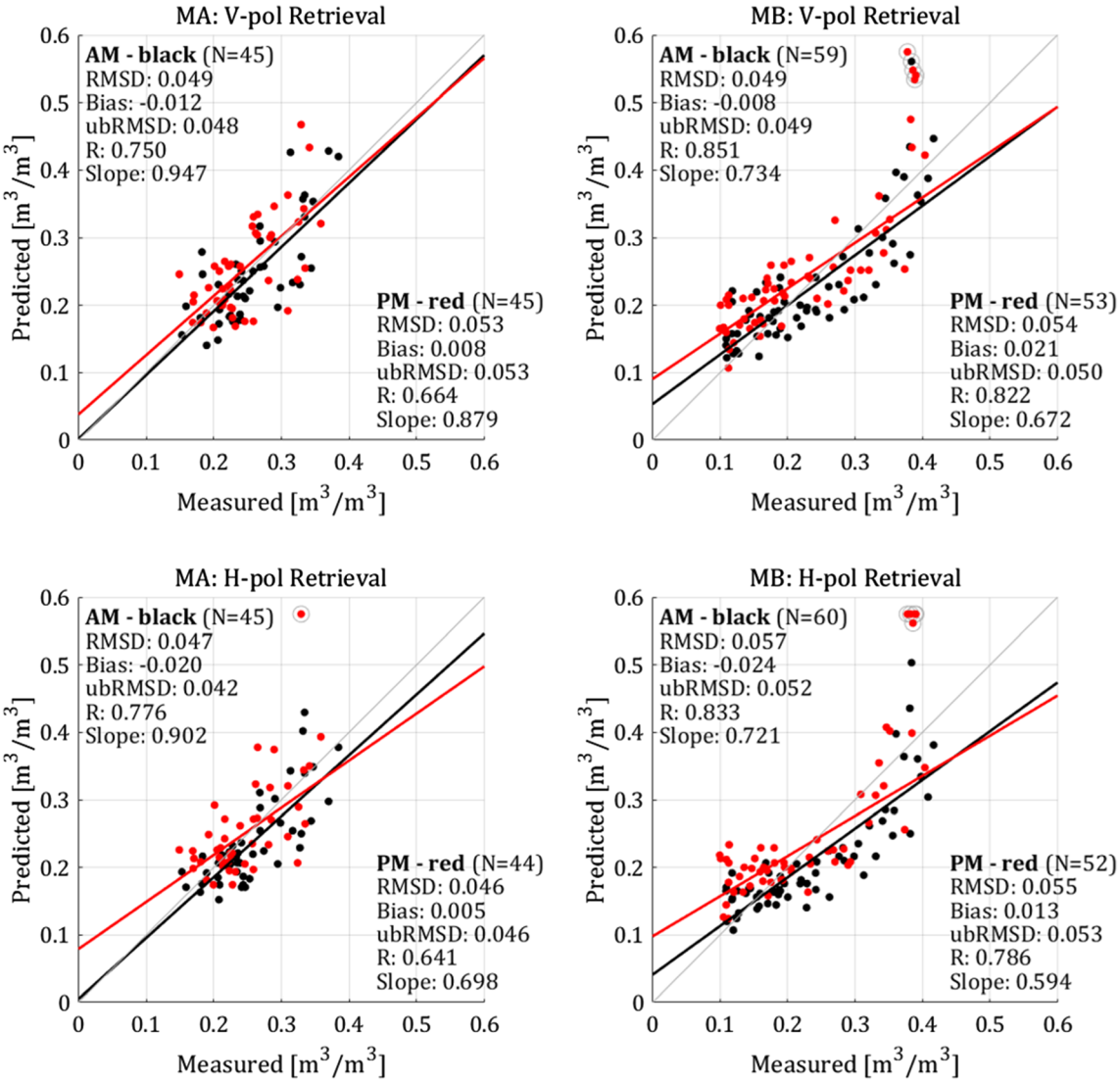

Figure 2. Scatterplots of the retrieved and reference soil moistures using vertical (top row) and horizontal (bottom row) polarizations for MA (left-hand side) and MB (right-hand side) pixels. The metrics show RMSD (m^3/m^3), bias (m^3/m^3), unbiased RMSD (ubRMSD) (m^3/m^3), and correlation (R) (-) (P values <0.01). The black dots represent the morning overpasses (AM), and the red dots represent the evening overpasses (PM). The circled data points are the early season outliers, which are not included in the metrics.

supporting information shows the time series of the measurements and retrievals and indicates also the timing of the outliers). We decided to remove these data points from the metrics computation because the conditions between snowmelt and leaf-on require further investigation, which is better studied using the multiyear time series that will be eventually collected in the experiment. The RMSD ranges from 0.047 to 0.057 m^3/m^3 for the AM overpasses and from 0.046 to 0.055 m^3/m^3 for the PM overpasses; the Pearson correlation ranges from 0.75 to 0.85 for the AM overpasses and 0.64 to 0.82 for the PM overpasses. The correlation is somewhat higher for AM than for PM but otherwise the differences between AM and PM metrics are small. The bias is negligible because we purposefully eliminated it by limiting it to ±1 in ε_r. For MB, the RMSD was higher for H polarization than for MA, but MB also had a larger range of soil moisture. Thus, despite the higher RMSD, MB had better correlations than MA in all cases. The metrics demonstrate that the SMAP measurements are sensitive to soil moisture under forest canopy at a reasonable precision.

The surface roughness parameter H_{0p} for each case was 0.51 for V polarization and 0.43 for H polarization, which translates to h_p of 1.15 and 1.44, respectively, and H_p of 0.67 and 0.84, respectively (see Table 1). These

Table 1
The Parameterization of the Retrieval Algorithm Used to Produce the Results in Figure 2 and the Parameter Values Used in the SMAP Single Channel Algorithm (SCA) for the Experiment Locations (O'Neill, Chan, Njoku, Jackson, & Bindlish, 2019)

		Surface roughness			Vegetation attenuation		Vegetation scattering		Vegetation absorption	SMAP SCA parameters		
Site	Pol	H_{0p}	h_p	H_p	t_p	τ_p	S_p	ω_p	a_p	h_p	τ_p	ω_p
MA	V	0.51	1.15	0.67	0.45	0.80	0.09	0.12	0.51	0.16	1.86	0.05
	H	0.43	1.44	0.84	0.59	0.53	0.05	0.10	0.38	0.16	1.86	0.05
MB	V	0.51	1.15	0.67	0.47	0.78	0.09	0.12	0.48	0.16	1.50	0.05
	H	0.43	1.44	0.84	0.61	0.49	0.06	0.12	0.35	0.16	1.50	0.05

values are significantly higher than that used by the SMAP in its SCA (0.16; see Table 1) and at the high end of roughness values reported in the literature, but not exceptionally high. Table 2 in Colliander et al. (2016) showed H_p values reported in several studies that ranged from 0.06 to 0.9.

Table 1 shows the vegetation parameter values obtained in the search process. For the attenuation, the table shows the values for both the t_p and τ_p, and for the scattering for both S_p and ω_p. The transmissivity is lower and scattering is higher for the V polarization for both sites. This is expected because the vertical structures of the forest interfere with the V polarization more effectively than with the H polarization. The transmissivity is somewhat lower for the MA pixel than for the MB pixel, which is in line with fact that the MB pixel contains more nonforested areas. The scattering parameters are very similar for both domains, and notably, ω_p is nearly uniform across all cases. Correspondingly, the absorption is larger for MA. As absorption of the vegetation determines the emission by the vegetation, the values indicate that at 20 °C temperature the vegetation TB contribution ($a_p \cdot T_{veg}$) would range from 40% to 55% of the total TB depending on the case. This result highlights the importance of compensating for the vegetation correctly with both transmission and scattering parameters using the right temperature. Table 1 also shows that the τ_p parameters are significantly lower and the ω_p parameters are higher than those used in the SMAP SCA. The current SMAP SCA parameterization results in overestimation and reduced sensitivity to soil moisture through the large τ_p parameter value (see Figure S1).

The temperature measured by the 5-cm depth (horizontally installed) soil moisture sensors were used for T_{soil} and the temperature measured by the vertically installed soil moisture sensors were used for T_{veg}. There was some variability in the results for the optimal temperature between the vertical sensor and 5-cm sensor, but the utilization of the same choice of temperatures for each case did not affect the overall results markedly. The choice of the temperature sources optimizes the parameter search together with the other parameters; this result alone does not directly indicate that these particular choices for the measurements would correspond most accurately to the real effective temperature of the soil and vegetation. As a practical example, the vegetation emission is a product of the absorption and the effective temperature (see above); parameters leading to a lower absorption could be compensated with a higher temperature and vice versa.

4. Discussion and Conclusion

In this letter, we took the first step toward quantifiably defined soil moisture retrieval for forests using spaceborne L-band radiometry. We used the SMAP TB measurements to achieve results that affirm the capability to retrieve soil moisture under the full canopy of temperate forests. The study focused on showing that we could find a set of emission model parameters that retrieve soil moisture with a reasonable performance from TB and physical temperature measurements. The V polarization RMSD to the in situ measurements were 0.049 and 0.054 m^3/m^3 over the MA and MB sites and correlation 0.66 and 0.85, respectively; the corresponding metrics for the H polarization were 0.046 and 0.57 m^3/m^3 for RMSD and 0.64 and 0.83 for correlation. The differences between polarizations and overpass times were not substantial. Traditionally, this level of performance has been considered as a sign of successful soil moisture retrieval.

One of the significant findings of the study was the general level of transmissivity through the forest vegetation layer. While the attenuation by the forest is considerable, it is not enough to entirely suppress the soil moisture signal. The selection of the vegetation transmission and scattering parameters is critical as well

as the use of a correct physical temperature for the estimation of the vegetation emission. Traditionally, AM overpasses have been favored for soil moisture retrieval because the temperature gradient between vegetation and soil tends to be smaller than later in the day (O'Neill, Chan, Njoku, Jackson, & Bindlish, 2019). However, the air and soil temperature measurements recorded in the experiment exhibited a seasonal change in the timing and magnitude of the gradient: The gradient was smaller during the AM overpasses in the spring, but toward the late summer, the gradient was, in fact, smaller during the PM overpasses (Figure S2). This explains the relative similarity of the metrics computed for the AM and PM retrievals and suggests PM observations may be more useful for soil moisture retrieval (if vegetation canopy temperature can be correctly accounted for) than traditionally considered.

The flip side of the relatively large vegetation attenuation is that the TB measurements also carry a great amount of information on the vegetation properties. In the past studies, the vegetation transmission for L-band TB has been related to the vegetation water content (Jackson & Schmugge, 1991; Kirdiashev et al., 1979). Recently, the vegetation optical depth in forests has been related to plant hydrology (Konings et al., 2019). This study supports this line of utilization of L-band TB measurements. However, the tuning process showed there are substantial differences between V and H polarizations. The commonly used algorithms for retrieving vegetation parameters assume the same transmission and scattering values for V and H (e.g., Chan et al., 2016; Chaubell et al., 2020; Konings et al., 2017; Njoku & Li, 1999). In light of this study, these algorithms may need to account for polarization differences for a better performance in the future.

This study focused on the first-year station-based soil moisture measurements from SMAPVEX19-21 to demonstrate the sensitivity of the spaceborne L-band TB to soil moisture. Eventually, the experiment will provide a very rich data set on both soil and vegetation properties with a longer time series that will enable more detailed investigations into both soil moisture and vegetation retrievals in temperate forest canopies.

Data Availability Statement

The SMAP data products (https://doi.org/10.5067/017XZSKMLTT2) and the station data (https://doi.org/10.5067/3LXL78PSKVXQ and https://doi.org/10.5067/NXNJWN9933UI) can be accessed through the National Snow and Ice Data Center (https://nsidc.org).

Acknowledgments

This work was performed at Jet Propulsion Laboratory, California Institute of Technology, under a contract with the National Aeronautics and Space Administration. We would like to thank Dr. Charles D. Canham for processing the U.S. Forest Service Forest Inventory and Analysis data. N. M. H. and A. G. K. were supported by NASA Terrestrial Ecology Award 80NSSC18K0715 through the New Investigator Program. USDA is an equal opportunity employer and provider.

References

Ahmed, R., Siqueira, P., Hensley, S., & Bergen, K. (2013). Uncertainty of forest biomass estimates in north temperate forests due to allometry: Implications for remote sensing. *Remote Sensing*, *5*(6), 3007–3036. https://doi.org/10.3390/rs5063007

Chan, S. K., Bindlish, R., O'Neill, P., Jackson, T., Njoku, E., Dunbar, S., et al. (2018). Development and assessment of the SMAP enhanced passive soil moisture product. *Remote Sensing of Environment*, *204*, 931–941. https://doi.org/10.1016/j.rse.2017.08.025

Chan, S. K., Bindlish, R., O'Neill, P. E., Njoku, E., Jackson, T., Colliander, A., et al. (2016). Assessment of the SMAP passive soil moisture product. *IEEE Transactions on Geoscience and Remote Sensing*, *54*(8), 4994–5007. https://doi.org/10.1109/TGRS.2016.2561938

Chaubell, J., Yueh, S. H., Peng, J., Dunbar, R. S., Chan, S. K., Chen, F., et al. (2019). Improving brightness temperature measurements near coastal areas for SMAP. *IEEE Journal of Selected Topics in Applied Earth Observations and Remote Sensing*, *12*(11), 4578–4588. https://doi.org/10.1109/JSTARS.2019.2951323

Chaubell, M. J., Yueh, S. H., Dunbar, R. S., Colliander, A., Chen, F., Chan, S. K., et al. (2020). Improved SMAP dual-channel algorithm for the retrieval of soil moisture. *IEEE Transactions on Geoscience and Remote Sensing*, *58*(6), 3894–3905. https://doi.org/10.1109/TGRS.2019.2959239

Chen, F., Crow, W. T., Cosh, M. H., Colliander, A., Asanuma, J., Berg, A., et al. (2019). Uncertainty of reference pixel soil moisture averages sampled at SMAP core validation sites. *Journal of Hydrometeorology*, *20*(8), 1553–1569. https://doi.org/10.1175/JHM-D-19-0049.1

Choat, B., Jansen, S., Brodribb, T. J., Cochard, H., Delzon, S., Bhaskar, R., et al. (2012). Global convergence in the vulnerability of forests to drought. *Nature*, *491*(7426), 752–755. https://doi.org/10.1038/nature11688

Choudhury, B. J., Schmugge, T. J., Chang, A., & Newton, R. W. (1979). Effect of surface roughness on the microwave emission from soils. *Journal of Geophysical Research*, *84*(C9), 5699–5706. https://doi.org/10.1029/JC084iC09p05699

Colliander, A., Cosh, M. H., Misra, S., Jackson, T. J., Crow, W. T., Chan, S., et al. (2017). Validation and scaling of soil moisture in a semi-arid environment: SMAP Validation Experiment 2015 (SMAPVEX15). *Remote Sensing of Environment*, *196*, 101–112. https://doi.org/10.1016/j.rse.2017.04.022

Colliander, A., Cosh, M. H., Misra, S., Jackson, T. J., Crow, W. T., Powers, J., et al. (2019). Comparison of high-resolution airborne soil moisture retrievals to SMAP soil moisture during the SMAP Validation Experiment 2016 (SMAPVEX16). *Remote Sensing of Environment*, *227*, 137–150. https://doi.org/10.1016/j.rse.2019.04.004

Colliander, A., Jackson, T. J., Bindlish, R., Chan, S., Das, N., Kim, S. B., et al. (2017). Validation of SMAP surface soil moisture products with core validation sites. *Remote Sensing of Environment*, *191*, 215–231. https://doi.org/10.1016/j.rse.2017.01.021

Colliander, A., Njoku, E. G., Huang, H., Tsang, L. (2018). Soil moisture retrieval using full wave simulations of 3-D Maxwell equations for compensating vegetation effects. Proc. IEEE Int. Geosci. Remote Sens. Symposium 2018.

Colliander, A., Njoku, E. G., Jackson, T. J., Chazanoff, S., McNairn, H., Powers, J., & Cosh, M. H. (2016). Retrieving soil moisture for non-forested areas using PALS radiometer measurements in SMAPVEX12 field campaign. *Remote Sensing of Environment*, *184*, 86–100. https://doi.org/10.1016/j.rse.2016.06.001

Corlett, R. T. (2016). The impacts of droughts in tropical forests. *Trends in Plant Science*, *21*(7), 584–593. https://doi.org/10.1016/j.tplants.2016.02.003

Cosh, M., Kelly, V., & Colliander, A. (2020a). SMAPVEX19–21 Massachusetts temporary soil moisture network, Version 1. Boulder, Colorado USA. NASA National Snow and Ice Data Center Distributed Active Archive Center. https://doi.org/10.5067/3LXL78PSKVXQ

Cosh, M., Kelly, V., & Colliander, A. (2020b). SMAPVEX19–21 Millbrook temporary soil moisture network, Version 1. Boulder, Colorado USA. NASA National Snow and Ice Data Center Distributed Active Archive Center. https://doi.org/10.5067/NXNJWN9933UI

Crow, W. T., Berg, A. A., Cosh, M. H., Loew, A., Mohanty, B. P., Panciera, R., et al. (2012). Upscaling sparse ground-based soil moisture observations for the validation of coarse-resolution satellite soil moisture products. *Reviews of Geophysics*, *50*, RG2002. https://doi.org/10.1029/2011RG000372

Dane, J. H., & Topp, G. C. (Eds.) (2002). *Methods of soil analysis part 4 physical methods*. Madison, WI: Soil Science Society of America. https://doi.org/10.2136/sssabookser5.4

Das, N., Entekhabi, D., Dunbar, R. S., Chaubell, M. J., Colliander, A., Yueh, S., et al. (2019). The SMAP and Copernicus Sentinel 1A/B microwave active-passive high resolution surface soil moisture product. *Remote Sensing of Environment*, *223*, 111380. https://doi.org/10.1016/j.rse.2019.111380

Djamai, N., Magagi, R., Goita, K., Hosseini, M., Cosh, M. H., Berg, A., & Toth, B. (2015). Evaluation of SMOS soil moisture products over the CanEx-SM10 area. *Journal of Hydrology*, *520*, 254–267. https://doi.org/10.1016/j.jhydrol.2014.11.026

Dorigo, W., Wagner, W., Albergel, C., Albrecht, F., Balsamo, G., Brocca, L., et al. (2017). ESA CCI soil moisture for improved Earth system understanding: State-of-the-art and future directions. *Remote Sensing of Environment*, *203*, 185–215. https://doi.org/10.1016/j.rse.2017.07.001

Doughty, C. E., Metcalfe, D. B., Girardinm, C. A. J., Farfan Amezquita, F., Galiano Cabrera, D., Huaraca Huasco, W., et al. (2015). Drought impact on Forest carbon dynamics and fluxes in Amazonia. *Nature*, *519*(7541), 78–82. https://doi.org/10.1038/nature14213

Entekhabi, D., Njoku, E. G., O'Neill, P. E., Kellogg, K. H., Crow, W. T., Edelstein, W. N., et al. (2010). The Soil Moisture Active Passive (SMAP) mission. *Proceedings of the IEEE*, *98*(5), 704–716. https://doi.org/10.1109/JPROC.2010.2043918

Entekhabi, D., Yueh, S., O'Neill, P., & Kellogg, K. (2014). *SMAP handbook—Soil moisture active passive: Mapping soil moisture and freeze/thaw from space*. Pasadena, CA: SMAP Project, Jet Propulsion Laboratory.

Famiglietti, J. S., Ryu, D., Berg, A. A., Rodell, M., & Jackson, T. J. (2008). Field observations of soil moisture variability across scales. *Water Resources Research*, *44*, W01423. https://doi.org/10.1029/2006WR005804

Ferrazzoli, P., Guerriero, L., & Wigneron, J.-P. (2002). Simulating L-band emission of forests in view of future satellite applications. *IEEE Transactions on Geoscience and Remote Sensing*, *40*(12), 2700–2708. https://doi.org/10.1109/TGRS.2002.807577

Guglielmetti, M., Schwank, M., Matzler, C., Oberdorster, C., Vanderborght, J., & Fluhler, H. (2008). FOSMEX: Forest soil moisture experiments with microwave radiometry. *IEEE Transactions on Geoscience and Remote Sensing*, *46*(3).

Jackson, T. J., & Schmugge, T. J. (1991). Vegetation effects on the microwave emission of soils. *Remote Sensing of Environment*, *36*(3), 203–212. https://doi.org/10.1016/0034-4257(91)90057-D

Kang, C. S., Kanniah, K. D., & Kerr, Y. H. (2019). Calibration of SMOS soil moisture retrieval algorithm: A case of tropical site in Malaysia. *IEEE Transactions on Geoscience and Remote Sensing*, *57*(6), 3827–3839. https://doi.org/10.1109/TGRS.2018.2888535

Kang, C. S., Kanniah, K. D., Kerr, Y. H., & Cracknell, A. P. (2016). Analysis of in-situ soil moisture data and validation of SMOS soil moisture products at selected agricultural sites over a tropical region. *International Journal of Remote Sensing*, *37*(16), 3636–3654. https://doi.org/10.1080/01431161.2016.1201229

Katz, D. S. W., Lovett, G. M., Canham, C. D., & O'Reilly, C. M. (2010). Legacies of land use history diminish over 22 years in a forest in Southeastern New York. *Journal of the Torrey Botanical Society*, *137*(2–3), 236–251. https://doi.org/10.3159/09-RA-038R1.1

Kerr, Y., Al-Yaari, A., Rodriguez-Fernandez, N., Parrens, M., Molero, B., Leroux, D., et al. (2016). Overview of SMOS performance in terms of global soil moisture monitoring after six years in operation. *Remote Sensing of Environment*, *180*, 40–63. https://doi.org/10.1016/j.rse.2016.02.042

Kirdiashev, K. P., Chukhlantsev, A. A., & Shutko, A. M. (1979). Microwave radiation of the Earth's surface in the presence of vegetation cover. *Radio Engineering and Electronics*, *24*, 256–264.

Konings, A. G., Piles, M., Das, N., & Entekhabi, D. (2017). L-band vegetation optical depth and effective scattering albedo estimation from SMAP. *Remote Sensing of Environment*, *198*, 460–470. https://doi.org/10.1016/j.rse.2017.06.037

Konings, A. G., Rao, K., & Steele-Dunne, S. C. (2019). Macro to micro: Microwave remote sensing of plant water content for physiology and ecology. *New Phytologist*, *223*(3), 1166–1172. https://doi.org/10.1111/nph.15808

Kurum, M., Lang, R. H., O'Neill, P. E., Joseph, A. T., Jackson, T. J., & Cosh, M. H. (2011). A first-order radiative transfer model for microwave radiometry of forest canopies at L-band. *IEEE Transactions on Geoscience and Remote Sensing*, *49*(9), 3167–3179. https://doi.org/10.1109/TGRS.2010.2091139

Kurum, M., O'Neill, P. E., Lang, R. H., Joseph, A. T., Cosh, M. H., & Jackson, T. J. (2012). Effective tree scattering and opacity at L-band. *Remote Sensing of Environment*, *118*, 1–9. https://doi.org/10.1016/j.rse.2011.10.024

Lang, R. H., Utku, C., de Matthaeis, P., Chauhan, N., & LeVine, D. M. (2001). ESTAR and model brightness temperatures over forests: Effects of soil moisture. Proc. IEEE Int. Geosci. Remote Sens. Symp. 2001.

Macelloni, G., Paloscia, S., Pampaloni, P., Ruisi, R., & Susini, C. (2001). Airborne multifrequency L- to Ka-band radiometric measurements over forests. *IEEE Transactions on Geoscience and Remote Sensing*, *39*(11), 2507–2513. https://doi.org/10.1109/36.964988

Matheny, A. M., Bohrer, G., Garrity, S. R., Morin, T. H., Howard, C. J., & Vogel, C. S. (2015). Observations of stem water storage in trees of opposing hydraulic strategies. *Ecosphere*, *6*(9), art165. https://doi.org/10.1890/ES15-00170.1

McNairn, H., Jackson, T., Wiseman, G., Belair, S., Berg, A., Bullock, P., et al. (2015). The Soil Moisture Active Passive Validation Experiment 2012 (SMAPVEX12): Pre-launch calibration and validation of the SMAP satellite. *IEEE Transactions on Geoscience and Remote Sensing*, *53*(5), 2784–2801. https://doi.org/10.1109/TGRS.2014.2364913

Mecklenburg, S., Drusch, M., Kaleschke, L., Rodriguez-Fernandez, N., Reul, N., Kerr, Y., et al. (2016). ESA's soil moisture and ocean salinity mission: From science to operational applications. *Remote Sensing of Environment*, *180*, 3–18. https://doi.org/10.1016/j.rse.2015.12.025

Mironov, V. L., Kosolapova, L. G., & Fomin, S. V. (2009). Physically and mineralogically based spectroscopic dielectric model for moisture soils. *IEEE Transactions on Geoscience and Remote Sensing*, *47*(7), 2059–2070.

Mo, T., Choudhury, B. J., Schmugge, T. J., Wang, J. R., & Jackson, T. J. (1982). A model for microwave emission from vegetation covered fields. *Journal of Geophysical Research*, *87*(C13), 11,229–11,237. https://doi.org/10.1029/JC087iC13p11229

Mohammed, P. N., Aksoy, M., Piepmeier, J. R., Johnson, J. T., & Bringer, A. (2016). SMAP L-band microwave radiometer: RFI mitigation prelaunch analysis and first year on-orbit observations. *IEEE Transactions on Geoscience and Remote Sensing*, *54*(10), 6035–6047. https://doi.org/10.1109/TGRS.2016.2580459

Monsiváis-Huertero, A., Hernández-Sánchez, J. C., Jiménez-Escalona, J. C., Galeana-Pizaña, J. M., Constantino-Recillas, D. E., Torres-Gómez, A. C., et al. (2020). Impact of temporal variations in vegetation optical depth and vegetation temperature on L-band passive soil moisture retrievals over a tropical forest using in-situ information. *International Journal of Remote Sensing*, *41*(6), 2098–2139. https://doi.org/10.1080/01431161.2019.1685715

Njoku, E. G., & Entekhabi, D. (1996). Passive microwave remote sensing of soil moisture. *Journal of Hydrology*, *184*(1–2), 101–129. https://doi.org/10.1016/0022-1694(95)02970-2

Njoku, E. G., & Kong, J.-A. (1977). Theory for passive microwave remote sensing of near-surface soil moisture. *Journal of Geophysical Research*, *82*(20), 3108–3118. https://doi.org/10.1029/JB082i020p03108

Njoku, E. G., & Li, L. (1999). Retrieval of land surface parameters using passive microwave measurements at 6–18 GHz. *IEEE Transactions on Geoscience and Remote Sensing*, *37*(1), 79–93. https://doi.org/10.1109/36.739125

O'Neill, P., Chan, S., Njoku, E. G., Jackson, T. J., Bindlish, R. (2019). Algorithm theoretical basis document level 2 & 3 soil moisture (passive) data products, Rev. E. SMAP Project, JPL D-66480, August 15, 2019. Jet Propulsion Laboratory, Pasadena, CA.

O'Neill, P. E., Chan, S., Njoku, E. G., Jackson, T., Bindlish, R., & Chaubell, J. (2019). SMAP enhanced L2 radiometer half-orbit 9 km EASE-grid soil moisture, Version 3. Boulder, Colorado USA. NASA National Snow and Ice Data Center Distributed Active Archive Center. https://doi.org/10.5067/017XZSKMLTT2. [Date Accessed: June 23, 2020]

Piepmeier, J. R., Focardi, P., Horgan, K. A., Knuble, J., Ehsan, N., Lucey, J., et al. (2017). SMAP L-band microwave radiometer: Instrument design and first year on orbit. *IEEE Transactions on Geoscience and Remote Sensing*, *55*(4), 1954–1966. https://doi.org/10.1109/TGRS.2016.2631978

Piepmeier, J. R., Johnson, J. T., Mohammad, P. N., Bradley, D., Ruf, C., Aksoy, M., et al. (2014). Radio-frequency interference mitigation for the soil moisture active passive microwave radiometer. *IEEE Transactions on Geoscience and Remote Sensing*, *52*(1), 761–775. https://doi.org/10.1109/TGRS.2013.2281266

Roy, A., Toose, P., Mavrovic, A., Pappas, C., Royer, A., Derksen, C., et al. (2020). L-band response to freeze/thaw in a boreal Forest stand from ground- and tower-based radiometer observations. *Remote Sensing of Environment*, *237*. https://doi.org/10.1016/j.rse.2019.111542

Schmugge, T. J., O'Neill, P. E., & Wang, J. R. (1986). Passive microwave soil moisture research. *IEEE Transactions on Geoscience and Remote Sensing*, *GE-24*(1), 12–22.

Schwank, M., Naderpour, R., & Matzler, C. (2018). "Tau-omega"—And two-stream emission models used for passive L-band retrievals: Application to close-range measurements over a forest. *Remote Sensing*, *10*(12), 1868. https://doi.org/10.3390/rs10121868

Seppanen, J., Kainulainen, J., Heiskanen, J., Praks, J., & Hallikainen, M. (2016). Measurements of boreal coniferous forest soil and humus with an airborne radiometer. *IEEE Transactions on Geoscience and Remote Sensing*, *9*(7), 3219–3228. https://doi.org/10.1109/jstars.2016.2532923

Vittucci, C., Ferrazzoli, P., Kerr, Y., Richaume, P., Guerriero, L., Rahmoune, R., & Vaglio Laurin, G. (2016). SMOS retrieval over forests: Exploitation of optical depth and tests of soil moisture estimates. *Remote Sensing of Environment*, *180*, 115–127. https://doi.org/10.1016/j.rse.2016.03.004

Vittucci, C., Ferrazzoli, P., Kerr, Y., Richaume, P., Veglio Laurin, G., & Guerriero, L. (2019). Analysis of vegetation optical depth and soil moisture retrieved by SMOS over tropical forests. *IEEE Geoscience and Remote Sensing Letters*, *16*(4), 504–508. https://doi.org/10.1109/LGRS.2018.2878359